James Barshinger
Krautkramer,
Lewistown, PA 17044

Joseph L. Rose
Mem. ASME
Engineering Science and Mechanics Department,
The Pennsylvania State University,
University Park, PA 16802
e-mail:jlresm@engr.psu.edu

Michael J. Avioli, Jr.
FBS, Inc.,
State College, PA 16801

Guided Wave Resonance Tuning for Pipe Inspection

Tremendous interest has surfaced recently on the use of guided waves in pipe inspection in the oil, chemical, and power generating industries. Relatively long lengths of piping can be inspected for corrosion and cracking from a single probe position. This saves a great deal of time and money compared to using more standard point-by-point normal beam inspection procedures. Pipes can be inspected without removing insulation or tar coatings by controlling the guided wave modes and frequencies used to carry out the study. This paper will review the history and state of the art of the guided wave techniques in piping. Benefits and limitations of the various methods will be pointed out along with a vision of future directions in the area of pipe inspection. [DOI: 10.1115/1.1491580]

Introduction

Interest in the guided wave inspection of pipes has peaked during the last decade because of the possibility of inspecting long lengths of pipe from a single probe position. The potential for inspection of pipes under insulation, soil, or tar, those embedded in concrete, and those generally hidden from sight is becoming realized. For general reading and a review on guided waves, see [1–6]. Textbooks containing fundamental topics in guided wave analysis can be found in [7–11]. Early work that serves as background in pipe analysis is presented in [12–30]. Recent published works on pipe inspection with guided waves can be found in [31–55]. The current thinking on wave resonance tuning to optimize defect detection, location, classifications, and sizing potential is introduced in [56–59]. Some computational techniques to assist the inspection process for defect classification and sizing analysis can be found in [60–63].

Material presented in this paper goes beyond earlier works and emphasizes the wave resonance tuning approach to defect analysis and improved penetration power. The wave tuning exercise is illustrated with a defect cluster detection experiment in a pipe followed by some analytical and experimental tuning of guided waves in a coal tar coated pipe. Excellent results were obtained.

Theory

In general, there are two basic methods for constructing multilayer waveguide solutions, the transfer matrix method [64,65], and the global matrix method [66]. Although, the global matrix method tends to be more computationally inefficient, it has the benefits of simplicity, and an inherent numerical stability that can be difficult to achieve in the transfer matrix method [4,64–67]. Thus, the global matrix method is used here to describe the multilayer, hollow cylinder waveguide. A schematic representation of the layer system is shown in Fig. 1.

The derivation begins with Navier's equation of motion (1), where $\mathbf{u}$ is the displacement field, λ and μ are the Lamé constants for the material, and ρ is the density, where the vector operations are performed in the cylindrical coordinate system. Due to the correspondence principle, it is not necessary to distinguish between elastic and viscoelastic layers [68]. Layers are considered elastic when the material constants are purely real numbers, while layers are visco-elastic when the material constants are complex.

$$\mu\nabla^2 u+(\lambda+\mu)\nabla(\nabla\cdot u)=\rho\frac{\partial^2 u}{\partial t^2} \tag{1}$$

Although Navier's equation is intractable in this form, it can be reduced into scalar and vector wave equations by the method of Helmholtz, (2), where the displacement field is assumed to be a combination of the gradient of a scalar potential field, Φ, and the curl of a vector potential field, $\mathbf{H}$, with the additional constraint that $\nabla\cdot\mathbf{H}=0$ [9].

$$\mathbf{u}=\nabla\Phi+\nabla\times\mathbf{H} \tag{2}$$

Thus, the resulting wave equations are (3) and (4), where (3) represents the longitudinal wave motion in the structure and (4) represents the shear wave motion; c_1 and c_2 are the longitudinal and shear wave velocities of the medium.

$$\nabla^2\Phi=\frac{1}{c_1^2}\frac{\partial^2\Phi}{\partial t^2},\quad c_1=\sqrt{(\lambda+2\mu)/\rho} \tag{3}$$

$$\nabla^2\mathbf{H}=\frac{1}{c_2^2}\frac{\partial^2\mathbf{H}}{\partial t^2},\quad c_2=\sqrt{\mu/\rho} \tag{4}$$

If Eqs. (3) and (4) are solved entirely, a theoretical solution will be developed that represents all modes of propagation in the hollow cylinder, including the axially symmetric, nonaxially symmetric and torsional guided wave modes [15,17]. However, the axially symmetric guided wave solution can be isolated by assuming that only the theta component of the vector potential field is nonzero and that both the vector and scalar potential fields are only functions of coordinates r and z [9]. Assuming time harmonic motion in the z coordinate direction, the solution of the scalar and vector wave equations is (5) and (6).

$$\Phi=\{A_{(L+)}\mathbf{H}_0^1(\alpha r)+A_{(L-)}\mathbf{H}_0^2(\alpha r)\}e^{i(kz-\omega t)} \tag{5}$$

$$\mathbf{H}=\{A_{(S+)}\mathbf{H}_1^1(\beta r)+A_{(s-)}\mathbf{H}_1^2(\beta r)\}e^{i(kz-\omega t)}e_\theta \tag{6}$$

The quantities involved in the solution are defined as follows: $A_{(L+)}$, $A_{(L-)}$, $A_{(S+)}$, $A_{(S-)}$, are the unknown amplitude constants for longitudinal and shear waves propagating in the layer in the outward and inward directions, ω is the angular frequency, k is the wave number, and α and β are given by (7). The functions $H_n^{1,2}(z)$ are the nth order Hankel functions of the first and second kind. Hankel functions are used instead of Bessel functions because they provide better numerical stability when seeking solutions in the range of phase velocities where individual wave components become nonpropagating across the layers.

$$\alpha^2=(\omega^2/c_1^2-k^2),\quad \beta^2=(\omega^2/c_2^2-k^2) \tag{7}$$

In order to construct the boundary conditions for the problem, it is necessary to make the layer matrix specific to a particular layer and interface. Inserting the appropriate elastic or viscoelastic material properties into the layer matrix, and inserting the radius of the boundary or interface that is being considered accomplishes

Contributed by the Pressure Vessels and Piping Division and presented at the Pressure Vessels and Piping Conference, Vancouver, Canada, August 4–8 2002, of THE AMERICAN SOCIETY OF MECHANICAL ENGINEERS. Manuscript received by the PVP Division, April 27, 2002. Associate Editor: S. Y. Zamrik.

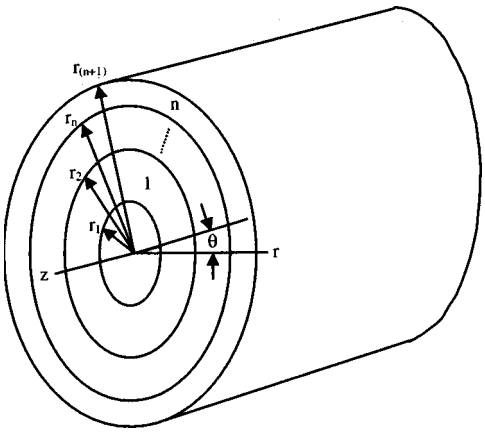

Fig. 1 Schematic representation of a multilayer hollow cylinder

this. The notation that is used here is to use subscripts to indicate the layer, and radius of the layer is being evaluated, such that $[\Lambda_{12}]$ is the layer matrix evaluated for the first layer at its outside radius as defined by Fig. 1. An additional matrix, $[\Gamma]$, is defined as the lower 2×4 submatrix of the layer matrix, $[\Lambda]$. This matrix is used to prescribe the boundary conditions on the free surfaces, where the displacement components of the layer matrix must be omitted. The specific boundary conditions for the problem are the vanishing of normal and shear stresses and the free surfaces of the problem, and the continuity of stress and displacement at the interfaces between layers. Using the matrix formalism of (8), each boundary condition for the problem can be prescribed. The total set of boundary conditions can then be constructed into a global matrix equation. For instance, the global matrix equation for a four-layer system is (9). This matrix contains the layer matrices for each layer, evaluated at the interfaces where a boundary condition is prescribed. The subvectors $\{A\}$ contain the unknown amplitude constants for the layers. The next step towards solving the boundary value problem for the multi-layer hollow cylinder is to generate the equations for the displacement and stress fields in the layer. The displacement field is generated by substituting the scalar and vector potential solutions into Eq. (2). The stress field is derived by consecutively applying the strain-displacement and stress-strain constitutive equations to the displacement field equations. The displacement and stresses are expressed in a matrix format as in (8), where $[\Lambda]$ is called the layer matrix.

$$\begin{Bmatrix} u_z \\ u_r \\ \sigma_{rr} \\ \sigma_{rz} \end{Bmatrix} = [\Lambda] \begin{Bmatrix} A_{(L+)} \\ A_{(L-)} \\ A_{(S+)} \\ A_{(S-)} \end{Bmatrix} e^{i(kz-\omega t)} \tag{8}$$

$$[\Lambda] = \begin{bmatrix} -\mathrm{k}\mathrm{H}_0^1(\alpha r) & -\mathrm{k}\mathrm{H}_0^2(\alpha r) & -\beta\mathrm{H}_0^1(\beta r) & -\beta\mathrm{H}_0^2(\beta r) \\ -\alpha\mathrm{H}_1^1(\alpha r) & -\alpha\mathrm{H}_1^2(\alpha r) & \mathrm{k}\mathrm{H}_1^1(\beta r) & \mathrm{k}\mathrm{H}_1^2(\beta r) \\ \mu\left((k^2-\beta^2)\mathrm{H}_0^1(\alpha r)+2\dfrac{\alpha}{r}\mathrm{H}_1^1(\alpha r)\right) & \mu\left((k^2-\beta^2)\mathrm{H}_0^2(\alpha r)+2\dfrac{\alpha}{r}\mathrm{H}_1^2(\alpha r)\right) & \mu\left(2k\beta\mathrm{H}_0^1(\beta r)-2\dfrac{k}{r}\mathrm{H}_1^1(\beta r)\right) & \mu\left(2k\beta\mathrm{H}_0^2(\beta r)-2\dfrac{k}{r}\mathrm{H}_1^2(\beta r)\right) \\ -2\mu\mathrm{k}\alpha\mathrm{H}_1^1(\alpha r) & -2\mu\mathrm{k}\alpha\mathrm{H}_1^2(\alpha r) & \mu(\mathrm{k}^2-\beta^2)\mathrm{H}_1^1(\beta r) & \mu(\mathrm{k}^2-\beta^2)\mathrm{H}_1^2(\beta r) \end{bmatrix}$$

$$\times \begin{bmatrix} (\Gamma_{11}) & 0 & 0 & 0 \\ [\Lambda_{12}] & [-\Lambda_{22}] & 0 & 0 \\ 0 & [\Lambda_{23}] & [-\Lambda_{33}] & 0 \\ 0 & 0 & [\Lambda_{34}] & [-\Lambda_{44}] \\ 0 & 0 & 0 & [\Lambda_{45}] \end{bmatrix} \begin{Bmatrix} \{A_1\} \\ \{A_2\} \\ \{A_3\} \\ \{A_4\} \end{Bmatrix} e^{i(kz-\omega t)} = 0 \tag{9}$$

To obtain a nontrivial solution for the problem, the determinant of the global matrix must equal zero, resulting in a dispersion equation for the layer system. Aside from the material constants for each layer, there exists a single independent variable of frequency, and a single dependent variable of wave number. A plot of the wave number roots versus, frequency yields the dispersion curve for the structure.

The roots of the dispersion equation can be real, imaginary, or complex [69]. For elastic waveguides, the roots will be either real or imaginary, where the real roots describe a wave mode that is propagating with no attenuation, and the imaginary roots describe non-propagating wave modes. Complex roots exist when material attenuation is included in the model. These roots describe a propagating wave mode that is attenuating with distance from the source [69]. This is the type of result that is of interest for viscoelastic or combination elastic/viscoelastic waveguides.

Numerical Results

The complex roots of the dispersion equation can be quite difficult to find, due to the fact that the absolute value of the equation changes over many orders of magnitude between roots. Thus, routines such as Müllers method that rely on the slope of the function, tend to extrapolate wildly, finding some roots, but not being able to find all of the roots for a particular frequency of interest. An alternative to traditional root finding routines, is to find the local minima of the absolute value of the dispersion equation [4]. Although the method is computationally inefficient, it tends to reliably find all of the roots of the dispersion equation.

The real and imaginary parts of the complex wave number roots of the dispersion equation can be converted into phase velocity and attenuation values from Eqs. (10)–(12). This alternative representation is important in that the phase velocity values can be directly tied to the means of generating the guided wave, and the attenuation values are directly useful for choosing modes to penetrate a coated structure. The plots of phase velocity versus frequency are termed phase velocity dispersion curves, while the plots of attenuation versus frequency are attenuation dispersion curves.

$$c_{ph} = \frac{\omega}{\mathrm{Re}(k)} \tag{10}$$

$$\alpha = \mathrm{Im}(k) \tag{11}$$

$$\mathrm{Attenuation}(dB/m) = 20\log_{10}(e^{-1000\alpha}) \tag{12}$$

Table 1 Elastic and viscoelastic material properties

Material	$\mathrm{Re}(c_1)$ (km/s)	$\mathrm{Im}(c_1)$ (km/s)	$\mathrm{Re}(c_2)$ (km/s)	$\mathrm{Im}(c_2)$ (km/s)	ρ (gm/cm^3)
Steel	5.90	0.00	3.19	0.00	7.80
Bitumen Coating	1.86	-0.08	0.73	-0.13	1.50

In order to calculate the dispersion equation for a particular system of layers, it is necessary to obtain the material constants for each of the materials involved. The material constants are the longitudinal and shear wave velocities, and the material density. For elastic layers, the wave velocities are purely real quantities, while for viscoelastic layers, the wave velocities have an imaginary component. The complex wave velocities for viscoelastic materials are seldom published so it is necessary to measure the quantities. This can be done by measuring velocity and attenuation of longitudinal and shear waves in the material [70]. The material properties for the elastic steel and viscoelastic bitumen coating are shown in Table 1. The phase velocity and attenuation dispersion curves for a 4-in. schedule 40 steel pipe, coated with 0.006 in. of bitumen are shown in Fig. 2.

The phase velocity dispersion curve looks quite typical as compared with dispersion curves for a single layer, elastic hollow cylinder. This is likely due to the fact that the viscoelastic coating is thin in comparison with the elastic layer. The attenuation dispersion curve is very interesting in that it shows drastic attenuation changes for the different modes over the frequency range of interest. The two lowest-order modes at low frequency show very good attenuation performance except at the point of the cutoff frequency for the $L(0,2)$ mode. As frequency increases the attenuation of the modes is tending to increase, although there are many specific points along the modes that have quite low attenuation values. These modes have great potential for performing a nondestructive test in a coated pipe.

Experimental Results on Defect Detection in a Clean Pipe

To illustrate the benefits of frequency tuning, a sample problem is given here. A hole defect and seven-hole cluster defect in a clean pipe were insonified with varying frequency. The peak-to-peak amplitude response for each frequency was measured and plotted as a function of frequency to identify any preferred frequency (ies). To perform the experiment, a Matec Explorer II™[1] tone-burst pulser/receiver was used with a 6-ft long 8-in. schedule 40 stainless steel pipe.

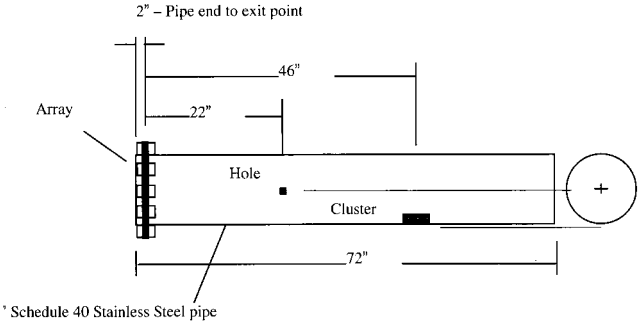

Fig. 3 Schematic of experimental arrangement showing hole and cluster locations relative to the ensemble exit point of the array

Figure 3 shows a schematic of the testing arrangement. Figure 4 shows the Matec Explorer II instrument and a view the 15-element array. Each array element has a 500-kHz transducer mounted on a Plexiglas shoe that is cut to provide a phase velocity of 0.116 in/μs or (2.95 mm/μs) and conforms to the curvature of the pipe. Figure 5 shows the "hole" defect and the "cluster" defect. Figure 6 shows the pipe, seven-hole cluster, and 15-element array.

Figure 7 shows the RF waveforms obtained from the hole defect and from the cluster defect. The main bang portion of the signals as well as the pipe end echo have been partially removed from the signals. The excitation frequency was varied from 100 to 675 kHz in 25-kHz increments. The gates indicate the hole position 22 in., and the cluster position 46 in. The bars to left and right show the peak-to-peak amplitude within the gates selected for the hole and for the cluster, respectively. Figures 8, and 9 show the bars transposed to a frequency axis slightly magnified for bet-

[1]Explorer II™ is a trademark of the Matec Corporation, Northbough, MA

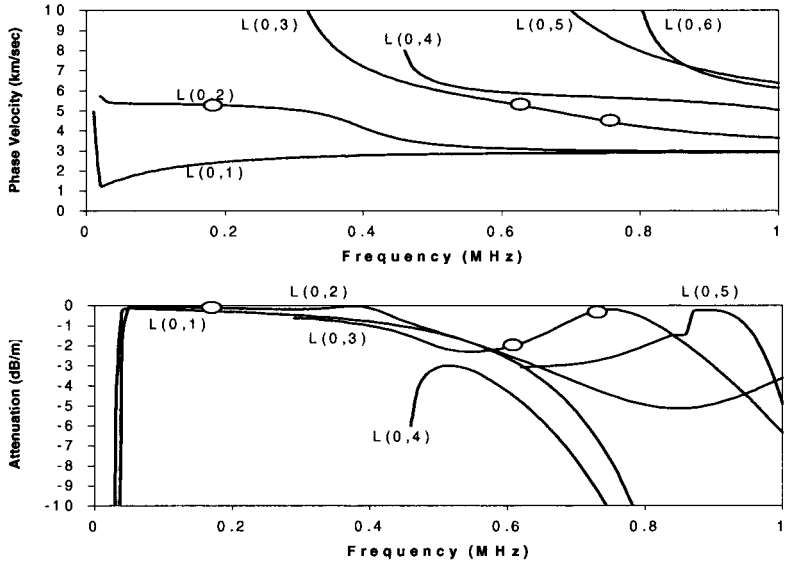

Fig. 2 Phase velocity and attenuation dispersion curves for a 4-in. schedule 40 steel pipe, coated with .006 in. of bitumen, showing the first six longitudinal modes of propagation

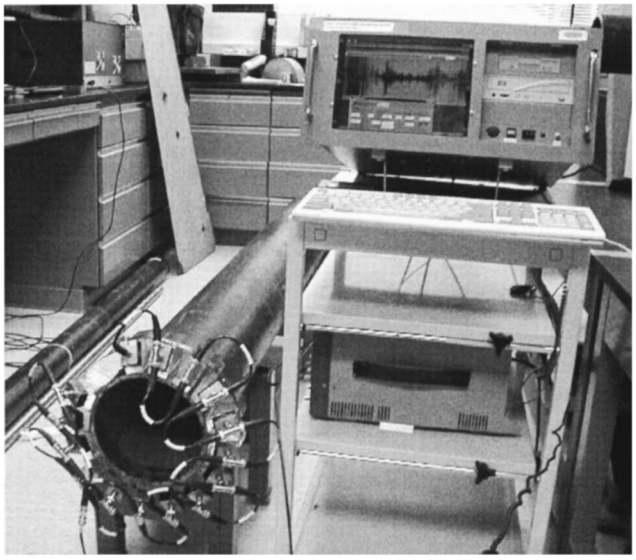

Fig. 4 Matec™ tone-burst pulser/receiver shown with test pipe

ter viewing. It is clear from these charts that frequency tuning can optimize the response from either the hole or the cluster. For example, and for this experiment 450 kHz produced the best amplitude response from the cluster and 125 kHz produced the best response from the hole.

Experimental Results From Defect Detection in a Coal Tar-Coated Pipe

In order to apply the knowledge gained from the attenuation dispersion curves, two test samples were prepared. Both samples consisted of a 10.5-ft length of 4-in. schedule 40 steel pipe with a transverse saw cut. The depth of the saw cut was made to 0.150 in. that produces a notch area that is equivalent to 5% of the total cross-sectional area of the pipe wall. A bitumen coating was applied to one of the test samples to an approximate thickness of 0.006 in.

Three modes were chosen from the attenuation dispersion curve to inspect the test samples: the $L(0,2)$ mode at 190 kHz, the $L(0,3)$ mode at 630 kHz, and the $L(0,3)$ mode at 740 kHz (see the circled modes on Fig. 2). From the attenuation dispersion curve, the expected result is that the $L(0,2)$ mode at 190 kHz, and the $L(0,3)$ mode at 740 kHz would be good choices for performing an inspection, while the $L(0,3)$ mode at 630 kHz would have unacceptably large attenuation. Figures 10–12 show the test results.

In all results, the echoes shown from left to right are as follows: 1) the initial excitation of the transducer; 2) the echo from the defect; and 3) the echo from the end of the pipe (BWE). The results are arranged in two columns, one for the clean pipe and one for the coated pipe. The upper results were taken with the same instrument gain to show a comparison of the actual signal strength of the defect and backwall for the two samples. For the lower results, the instrument gain was adjusted to bring the defect signal to 80% of full screen height. Then the defect signal strength can be compared with the baseline noise of the system to see if there was enough strength to resolve the defect from the noise.

As expected, the result showing the least amount of attenuation was the $L(0,2)$ mode at 190 kHz. The gain and signal to noise of the defect was quite similar for both the clean and coated pipes. The results for the $L(0,3)$ mode at 630 kHz are generally unacceptable from a nondestructive point of view, because the signal strength is almost entirely attenuated. Increasing the frequency of excitation to 740 kHz, the $L(0,3)$ again becomes usable, showing some attenuation, but still having excellent signal to noise on the defect. In fact, even though the frequency of operation has almost quadrupled from 190 to 740 kHz, the attenuation and signal to noise of the tests are very similar. Additionally, an interesting observation is that the back-wall is reduced in amplitude from the uncoated case. This is most likely due to mode conversion effects and not due to the presence of the coating. This result demonstrates the importance of having knowledge of the attenuation characteristics of guided waves propagating in a coated structure.

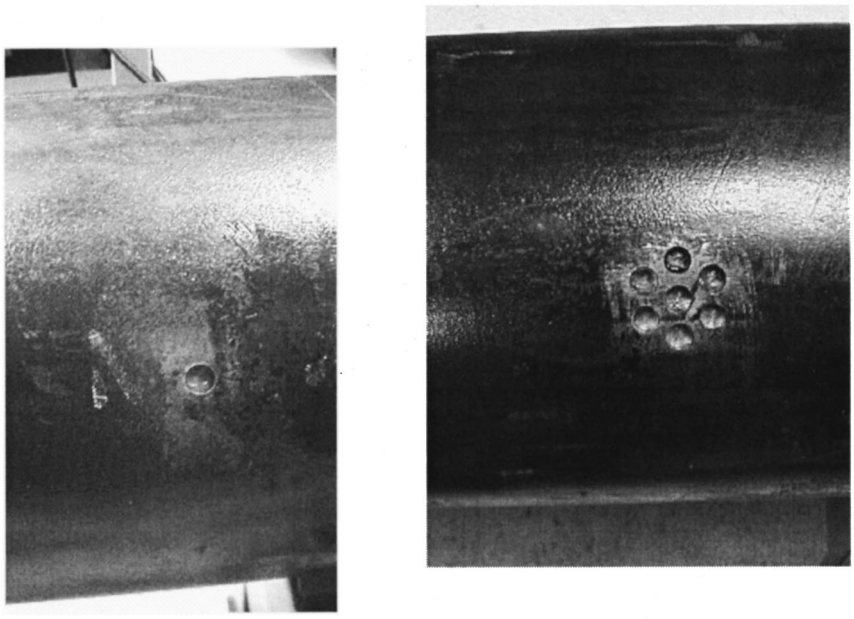

(*a*) (*b*)

Fig. 5 (*a*) Round bottom-hole defect (the diameter is 0.375 in. and the depth is 0.25 in.); (*b*) seven-hole cluster defect

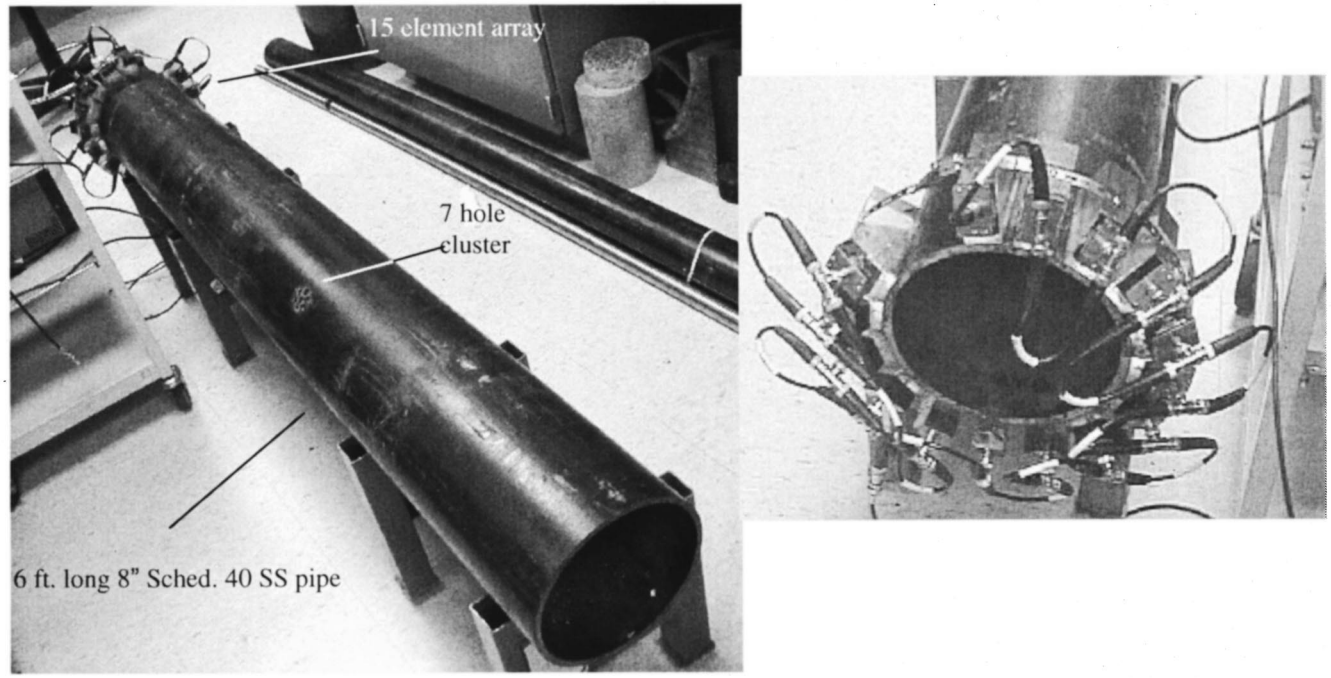

(*a*) (*b*)

Fig. 6 (*a*) End-on view of pipe showing location of seven-hole cluster; (*b*) view of 15-element array

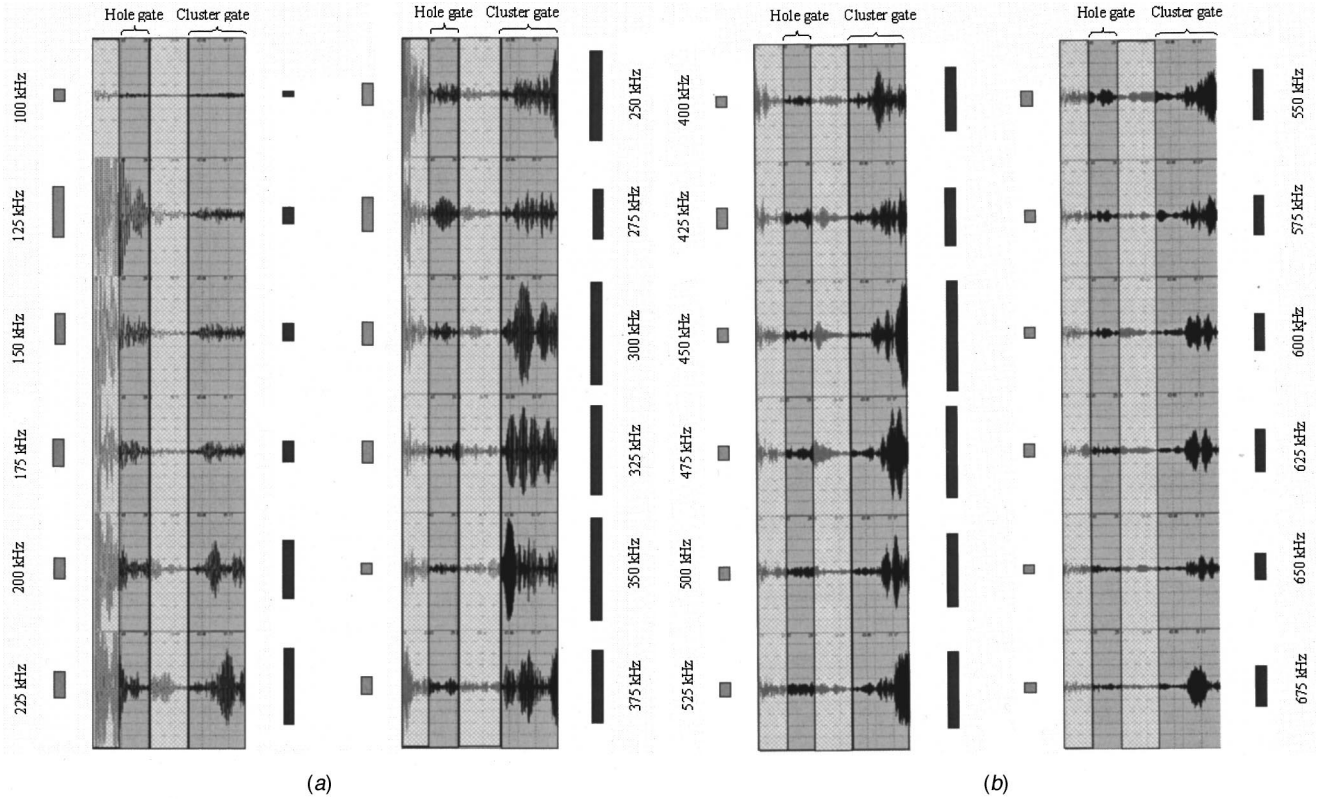

(*a*) (*b*)

Fig. 7 Gated RF waveforms from hole (left) and seven-hole cluster (right); medium gray bars are peak-to-peak values in the "hole" gate and the darker bars are peak-to-peak values in the "cluster" gate (on the right and left sides of the RF waveforms, respectively)—(*a*) frequency range (100, 375) kHz; (*b*) frequency range (400, 675) kHz

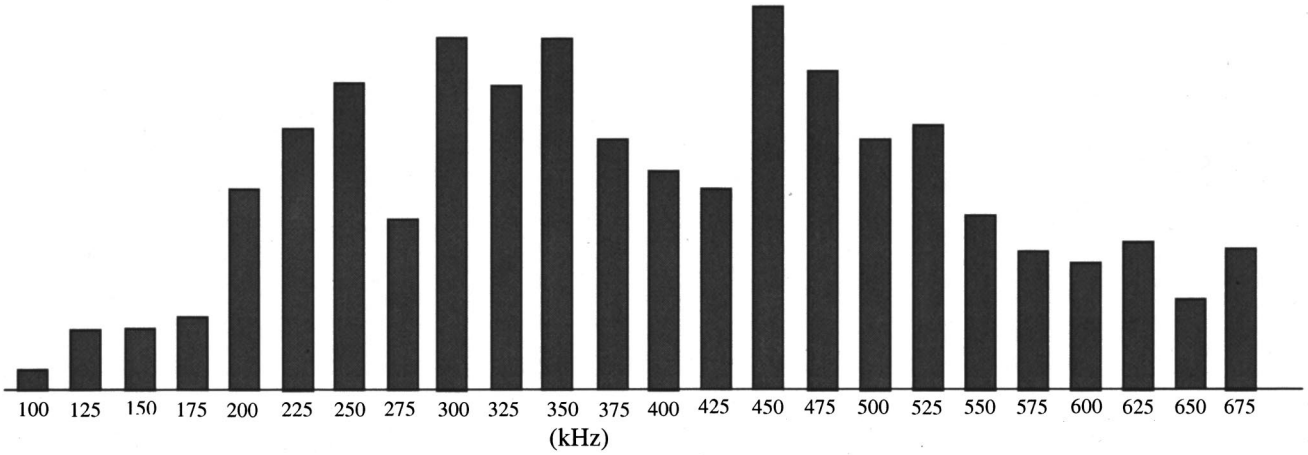

Fig. 8 Amplitude versus frequency distribution of echoes from seven-hole cluster

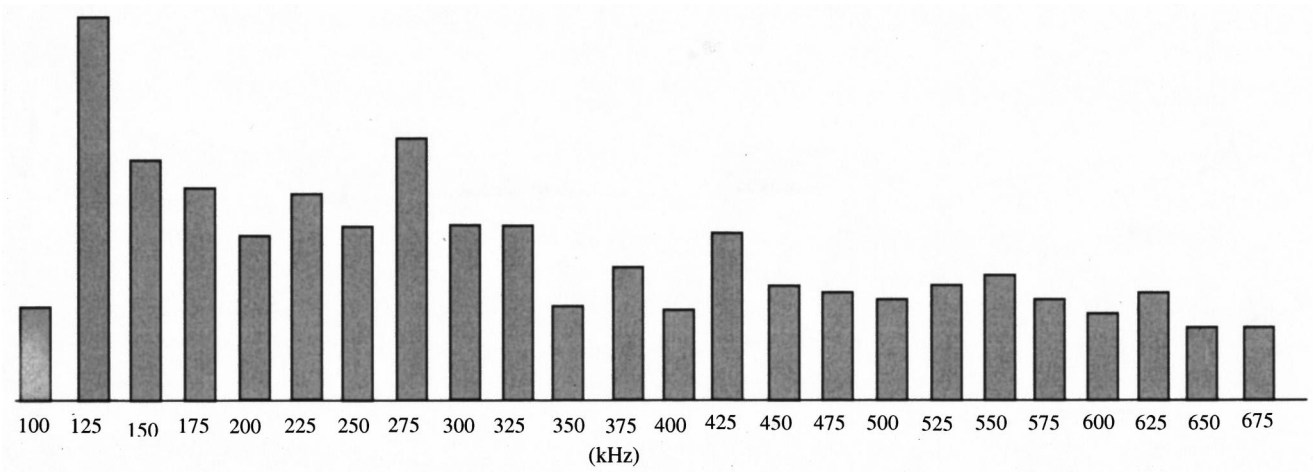

Fig. 9 Amplitude versus frequency distribution of echoes from lone hole

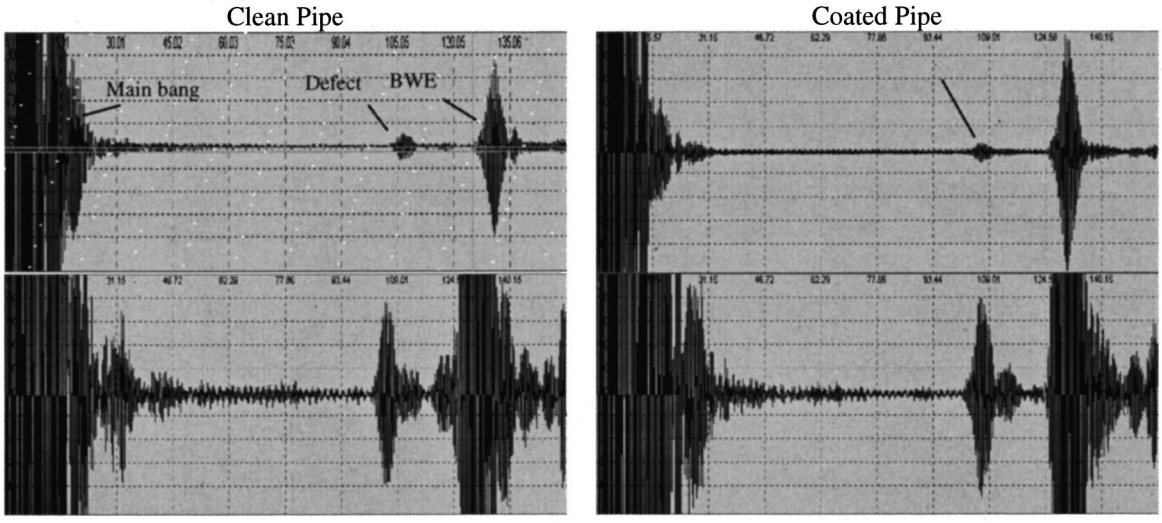

Fig. 10 Test results for a clean and coated pipe with a transverse notch of 5% cross-sectional area using the $L(0,2)$ mode at 190 kHz for inspection. The upper waveforms show the defect and back wall results for an equivalent instrument gain to demonstrate the attenuation difference between clean and coated test samples. The lower waveforms show the result when the instrument gain is adjusted to bring the notch to 80% of full screen height to demonstrate the difference in signal to noise of the test for clean and coated test samples. Despite the coating, excellent results are obtained.

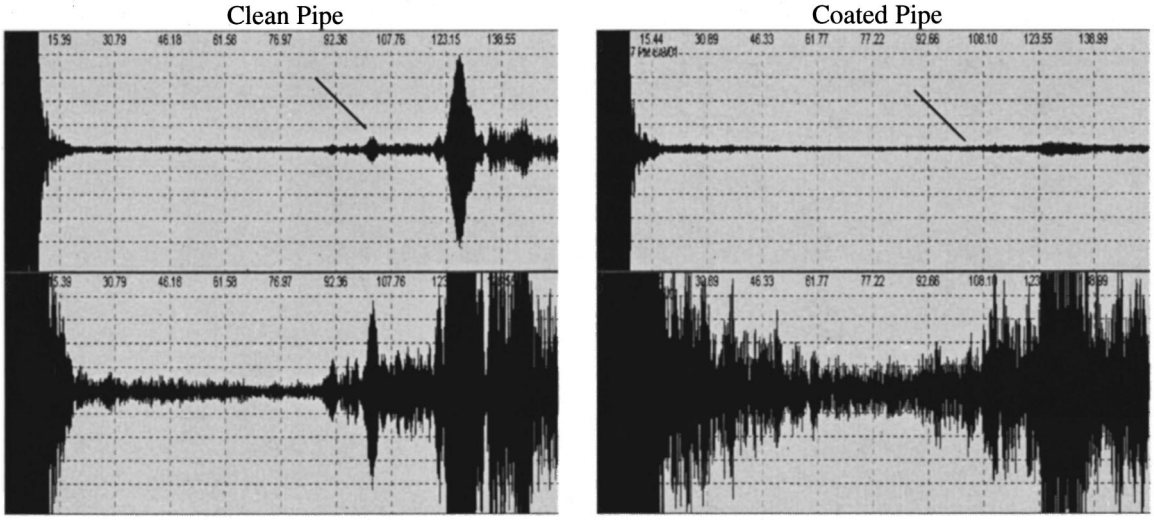

Fig. 11 Test results for a clean and coated pipe with a transverse notch of 5% cross-sectional area using the $L(0,3)$ mode at 630 kHz. The upper waveforms show the defect and back wall results for an equivalent instrument gain to demonstrate attenuation differences between clean and coated test samples. The lower waveforms show the result when the instrument gain is adjusted to bring the notch to 80% full screen height to show the difference in signal to noise of the test for clean and coated test samples. Poor results are obtained because of the coated pipe and improper mode and frequency selection.

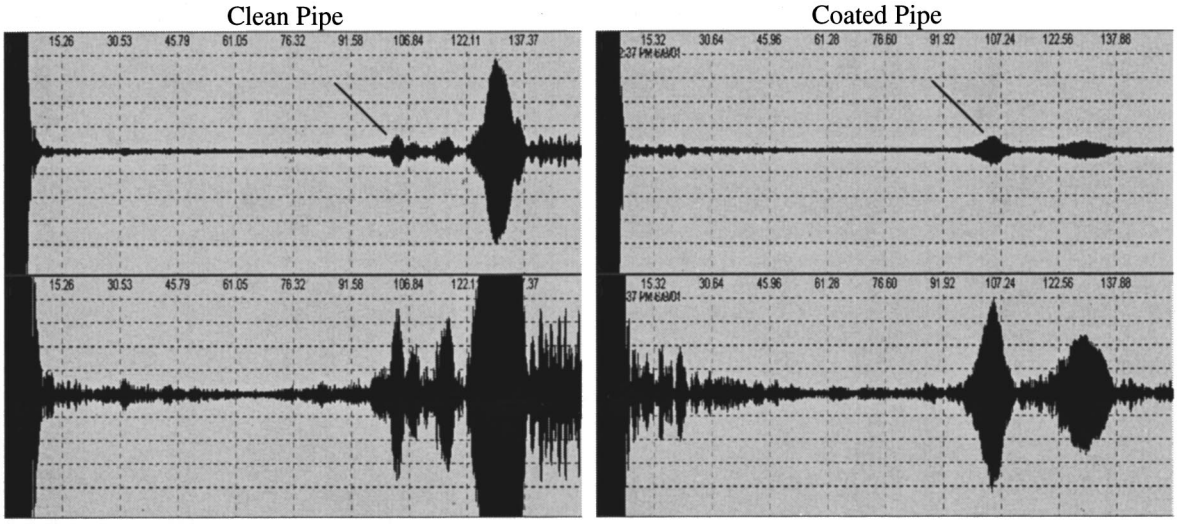

Fig. 12 Test results for a clean and coated pipe with a transverse notch of 5% cross-sectional area using the $L(0,3)$ mode at 740 kHz for inspection. The upper waveforms show the defect and back wall results for an equivalent instrument gain to demonstrate the attenuation difference between clean and coated test samples. The lower waveforms show the result when the instrument gain is adjusted to bring the notch to 80% of full screen height to demonstrate the difference in signal to noise of the test for clean and coated test samples. Despite the coating, excellent results are obtained.

It is now quite obvious that there are many low attenuation modes to choose beyond the $L(0,2)$ mode at low frequency.

Concluding Remarks

Great potential exists for the guided wave inspection of piping over long distances from a single probe position. Phase velocity and frequency wave resonance tuning, however, are often essential. Results for a set fixed phase velocity and frequency are not dependable. As a result of tuning, it becomes possible to improve penetration power despite coatings on the pipe and also to be able to detect difficult defect shapes. Theoretical and experimental results show that many choices of mode and frequency can be made to produce a good result. Quite often higher frequencies can have much better penetration power than lower frequencies.

References

[1] Chimenti, D. E., Nayfeh, A. H., and Butler, D. L., 1982, ''Leaky Waves on a Layered Half-Space,'' J. Appl. Phys., **53**, pp. 170–176.
[2] Ditri, J., Rose, J. L., and Chen, G., 1991, ''Mode Selection Guidelines for Defect Detection Optimization Using Lamb Waves,'' Proc., 18th Annual Review of Progress in Quantitative NDE Meeting, Plenum, Vol. 11, pp. 2109–2115, Brunswick, ME.
[3] Fortunko, C. M., King, R. B., and Tan, M., 1982, ''Nondestructive Evaluation of Planar Defects in Plates Using Low-Frequency Shear Horizontal Waves,'' J. Appl. Phys., **53**, pp. 3450–3458.

[4] Lowe, M. J. S., 1995, ''Matrix Techniques for Modeling Ultrasonic Waves in Multilayered Media,'' IEEE Trans. Ultrason. Ferroelectr. Freq. Control, **42**, pp. 525–542.
[5] Rokhlin, S., 1979, ''Interaction of Lamb Waves with Elongated Delaminations in Thin Sheets,'' Int. Adv. Nondestr. Test., **6**, pp. 263–285.
[6] Rose, J. L., 2002, ''Standing on the Shoulders of Giants-An Example of Guided Wave Inspection,'' Mehl Honor Lecture, Mater. Eval., **60**, pp. 53–59.
[7] Achenbach, J. D., 1984, *Wave Propagation in Elastic Solids*. North-Holland Publishing Co., New York.
[8] Auld, B. A., 1990, *Acoustic Fields and Waves in Solids*, Vol. 1 and 2, Second Edition.: Kreiger Publishing Co., FL.
[9] Graff, K. F., 1991, *Wave Motion in Elastic Solids*, Dover Publications Inc., New York, NY.
[10] Rose, J. L., 1999, *Ultrasonic Waves in Solid Media*, Cambridge University Press, New York, NY.
[11] Viktorov, I. A., 1967, *Rayleigh and Lamb Waves—Physical Theory and Applications*, Plenum Press, New York, NY.
[12] Armenkaas, Gazis, D. C., Herrmann, G., 1969, *Free Vibrations of Circular Cylindrical Shells*, Pergamon Press, New York, NY.
[13] Cooper, R. M., and Naghdi, P. M., 1957, ''Propagation of Nonaxially Symmetric Waves in Elastic Cylindrical Shells,'' J. Acoust. Soc. Am., **29**, pp. 1365–1373.
[14] Fitch, A. H., 1963, ''Observation of Elastic Pulse Propagation in Axially Symmetric and Nonaxially Symmetric Longitudinal Modes of Hollow Cylinders,'' J. Acoust. Soc. Am., **35**, pp. 706–707.
[15] Gazis, D. C., 1959, ''Three-Dimensional Investigation of the Propagation of Waves in Hollow Circular Cylinders, I. Analytical Foundation,'' J. Acoust. Soc. Am., **31**, pp. 568–573.
[16] Barshinger, J. N., Rose, J. L., 2001, ''Ultrasonic Guided Wave Propagation in Pipes With Viscoelastic Coatings,'' QNDE. Brunswick, ME, July 29-August 3.
[17] Gazis, D. C., 1959, ''Three-Dimensional Investigation of the Propagation of Waves in Hollow Circular Cylinders, II. Numerical Results,'' J. Acoust. Soc. Am., **31**, pp. 573–578.
[18] Cho, Y., and Rose, J. L., 1996, ''Guided Waves in a Water Loaded Hollow Cylinder,'' J. Nondestructive Testing & Evaluation, **12**, pp. 323–339.
[19] Ghosh, J., 1923–1924, ''Longitudinal Vibrations of a Hollow Cylinder,'' Bulletin of the Calcutta Mathematical Society, Bull. Calcutta Math. Soc., **14**, pp. 31–40.
[20] Greenspon, J. E., 1961, ''Vibrations of Thick and Thin Cylindrical Shells Surrounded by Water,'' J. Acoust. Soc. Am., **33**, pp. 1321–1328.
[21] Greenspon, J. E., 1959, ''Vibrations of Thick Cylindrical Shells,'' J. Acoust. Soc. Am., **31**, pp. 1682–1683.
[22] Herrmann, G., and Mirsky, I., 1956, ''Three-Dimensional and Shell-Theory Analysis of Axially Symmetric Motions of Cylinders,'' ASME J. Appl. Mech., **78**, pp. 563–568.
[23] Meeker, T. R., and Meitzler, A. H., 1964, ''Guided Wave Propagation in Elongated Cylinders and Plates,'' Phys. Acoust., **1A**, pp. 111–167.
[24] Mirsky, I., and Herrmann, G., 1976, ''Axially Symmetric Motions of Thick Cylindrical Shells,'' ASME J. Appl. Mech. **80**, pp. 97–102.
[25] Mohr, W., and Holler, P., 1976, ''On Inspection of Thin-Walled Tubes for Transverse and Longitudinal Flaws by Guided Ultrasonic Waves,'' IEEE Trans. Sonics Ultrason., **SU-23**, No. 5, pp. 369–374.
[26] Pao, Y. H., and Mindlin, R. D., 1960, ''Dispersion of Flexural Waves in an Elastic Circular Cylinder,'' ASME J. Appl. Mech., **27**, pp. 513–520.
[27] Silk, M. G., and Bainton, K. P., 1979, ''The propagation in Metal Tubing of Ultrasonic Wave Modes Equivalent to Lamb Waves,'' Ultrasonics, **17**, pp. 11–19.
[28] Thompson, R. B., Alers, G. A., and Tennison, M. A., 1972, ''Applications of Direct Electromagnetic Lamb Wave Generation to Gas Pipeline Inspection,'' IEEE Ultrasonics Symposium, pp. 91–94.
[29] Viktorov, I. A., 1958, ''Rayleigh-Type Waves on a Cylindrical Surface,'' Soviet Phys.-Acoust., **4**, pp. 131–136.
[30] Zemanek, J., Jr., 1972, ''An Experimental and Theoretical Investigation of Elastic Wave Propagation in a Cylinder,'' J. Acoust. Soc. Am., **51**, pp. 265–283.
[31] Alleyne, D. N., Pavlakovic, B., Lowe, M. J. S., and Cawley, P., 2001, ''Rapid Long-Range Inspection of Chemical Plant Pipework Using Guided Waves,'' Insight, **43**, pp. 93–96.
[32] Alleyne, D. N., Lowe, M. J. S., and Cawley, P., 1998, ''The Reflection of Guided Waves From Circumferential Notches in Pipes,'' ASME J. Appl. Mech., **65**, pp. 635–641.
[33] Alleyne, D. N., and Cawley, P., 1997, ''Long Range Propagation of Lamb Wave in Chemical Plant Pipework,'' Mater. Eval., **45**, pp. 504–508.
[34] Alleyne, D. N., and Cawley, P., 1996, ''The Excitation of Lamb Waves in Pipes Using Dry-Coupled Piezoelectric Transducers,'' J. Nondestruct. Eval., **15**, pp. 11–20.
[35] Ditri, J. J., 1994, ''Utilization of Guided Waves for the Characterization of Circumferential Cracks in Hollow Cylinders,'' J. Acoust. Soc. Am., **96**, pp. 3769–3775.
[36] Ditri, J. J., and Rose, J. L., 1992, ''Excitation of Guided Elastic Wave Modes in Hollow Cylinders by Applied Surface Tractions,'' J. Appl. Phys., **72**, pp. 2589–2597.
[37] Ditri, J., Rose, J., and Pilarski, A., 1992, ''Generation of Guided Waves in Hollow Cylinders by Wedge and Comb Type Transducers,'' *Review of Progress in Quantitative Nondestructive Evaluation*, eds., D. O. Thompson and D. Chimenti, Rev. Prog. Quant. Nondestr. Eval., **12A**, pp. 211–218.
[38] Guo, D., and Kundu, T., 2000, ''A New Sensor for Pipe Inspection by Lamb Waves,'' Mater. Eval., **58**, pp. 991–994.
[39] Kley, M., Valle, C., Jacobs, L. J., Qu, J., and Jarzynski, J., 1999, ''Development of Dispersion Curves for Two Layered Cylinders Using Laser Ultrasonics,'' J. Acoust. Soc. Am., **106**, pp. 582–588.
[40] Kwun, H., Dynes, H., 1998, ''Long Range Guided Wave Inspection of Pipe Using the Magnetostrictive Sensor Technology-Feasibility of Defect Characterization,'' International Society for Optical Engineering (SPIE) on Nondestructive Evaluation of Utilities and Pipelines II, **3398**, pp. 28–34.
[41] Li, J., and Rose, J. L., 2001a, ''Excitation and Propagation of Non-Axisymmetric Guided Waves in a Hollow Cylinder,'' J. Acoust. Soc. Am., **109**, pp. 457–464.
[42] Liu, G., and Qu, J., 1998, ''Transient Wave Propagation in a Circular Annulus Subjected to Impulse Excitation on its Outer Surface,'' J. Acoust. Soc. Am., **104**, pp. 1210–1220.
[43] Lowe, M. J. S., Alleyne, D. N., and Cawley, P., 1998, ''The Mode Conversion of a Guided Wave by a Part-Circumferential Notch in a Pipe,'' ASME J. Appl. Mech., **65**, pp. 649–656.
[44] Liu, G., and Qu, J., 1998, ''Guided Circumferential Waves in a Circular Annulus,'' ASME J. Appl. Mech., **65**, pp. 424–430.
[45] Mudge, P. J., 2001, ''Field Application of the Teletest Long-Range Ultrasonic Testing Technique,'' Insight, **43**, pp. 74–77.
[46] Nagy, P. B., Blodgett, M., and Gulis, M., 1994, ''Weep Hole Inspection by Circumferential Creeping Waves,'' NDT&E Int. **27**, pp. 131–142.
[47] Qu, J., Berthelot, Y., and Jacobs, L., 2000, ''Crack Detection in Thick Annular Components Using Ultrasonic Guided Waves,'' Proc. Instrn. Mech. Engrs. Part C, **214**, pp. 1163–1171.
[48] Quarry, M., and Rose, J. L., 1999, ''Multimode Guided Wave Inspection of Piping Using Comb Transducers,'' Mater. Eval., **57**, pp. 1089–90.
[49] Rose, J. L., and Zhao, X., 2001b, ''Anomaly Throughwall Depth Measurement Potential With Shear Horizontal Guided Waves,'' Mater. Eval., **59**, pp. 1234–1238.
[50] Rose, J. L., and Zhao, X., 2001c, ''Flexural Mode Tuning for Pipe Elbow Inspection,'' Mater. Eval., **59**, pp. 621–624.
[51] Rose, J. L., Jiao, D., and Spanner, J., Jr., 1996, ''Ultrasonic Guided Wave NDE for Piping,'' Mater. Eval., **54**, pp. 1310–1313.
[52] Rose, J. L., Rajana, K., and Carr, F., 1994b, ''Ultrasonic Guided Wave Inspection Concepts for Steam Generator Tubing,'' Mater. Eval., **52**, pp. 307–311.
[53] Shin, H. J., Rose, J. L., 1998, ''Non-Axisymmetric Ultrasonic Guided Waves in Pipes,'' 7th Annual Research Symposium, 1998 ASNT Spring Conference, Anaheim, CA, March 23–27.
[54] Valle, C., Niethammer, M., Qu, J., and Jacobs, L. J., 2001, ''Crack Characterization Using Guided Circumferential Waves,'' J. Acoust. Soc. Am., **109**, pp. 1841–1847.
[55] Valle, C., Qu, J., and Jacobs, L. J., 1999, ''Guided Circumferential Waves in Layered Cylinders,'' Int. J. Eng. Sci., **37**, pp. 1369–1387.
[56] Li, J., and Rose, J. L., 2001b, ''Implementing Guided Wave Mode Control by Use of a Phased Transducer Array,'' IEEE Trans. Ultrason. Ferroelectr. Freq **48**, pp. 761–768.
[57] Shin, H. J., Rose, J. L., 1998, ''Guided Wave Tuning Principles for Defect Detection in Tubing,'' J. Nondestruct. Eval., **17**, pp. 27–36.
[58] Wooh, S. C., and Shi, Y., 2001, ''Synthetic Phase Tuning of Guided Waves,'' IEEE Trans. Ultrason. Ferroelectr. Freq, **48**, pp. 209–223.
[59] Zhu, W., and Rose, J. L., 1999, ''Lamb Wave Generation and Reception With Time-Delay Periodic Linear Arrays: A BEM Simulation and Experimental Study,'' IEEE Trans. Ultrason. Ferroelectr. Freq., **46**, pp. 654–664.
[60] Alleyne, D. N., and Cawley, P., 1992, ''The Interaction of Lamb Waves With Defects,'' IEEE Trans. Ultrason. Ferroelectr. Freq., **39**, pp. 381–396.
[61] Chang, Z., and Mal, A., 1998, ''Wave Propagation in a Plate with defects,'' *Review of Progress in Quantitative Nondestructive Evaluation*, Rev. Prog. Quant. Nondestr. Eval., **17**, pp. 121–128.
[62] Cho, Y., and Rose, J. L., 1996, ''A Boundary Element Solution for a Mode Conversion Study on the Edge Reflection of Lamb Waves,'' J. Acoust. Soc. Am., **99**, pp. 2097–2109.
[63] Datta, S. K., Al-Nassar, Y., and Shah, A. K., 1991, ''Lamb Wave Scattering by a Surface Breaking Crack in a Plate,'' Review of Progress in Quantitative Nondestructive Evaluation, eds., D. O. Thompson and D. Chimenti, Rev. Prog. Quant. Nondestr. Eval., **10**, pp. 97–104.
[64] Thomson, W. T., 1950, ''Transmission of Elastic Waves Through Stratified Solid Medium,'' J. Appl. Phys., **21**, pp. 89–93.
[65] Haskell, N. A., 1953, ''Dispersion of Surface Waves on Multilayered Media,'' Bull. Seismol. Soc. Am., **43**, pp. 17–34.
[66] Knopoff, L., 1964, ''A Matrix Method for Elastic Wave Problems,'' Bull. Seismol. Soc. Am., **54**, pp. 431–438.
[67] Mal, Yin, and Bar Cohen, 1991, *Comps. Engra*., Vol. 1, pp. 85–101.
[68] Christensen, R. M., 1981, *Theory of Viscoelasticity: An Introduction*, Academic Press, New York, NY.
[69] Watson, T. H., 1972, ''A Real Frequency, Complex Wave-Number Analysis of Leaking Modes,'' Bull. Seismol. Soc. Am., **62**, pp. 369–384.
[70] Blanc, R. H., 1993, ''Transient Wave Propagation Methods for Determining the Viscoelastic Properties of Solids,'' ASME J. Appl. Mech., **60**, pp. 763–768.